This is a preprint, the final version is subject to change, of the American Mineralogist (MSA)
Cite as Authors (Year) Title. American Mineralogist, in press.
DOI: https://doi.org/10.2138/am-2019-6951

REVISION 2

Submission to the "American Mineralogist"

(An invited contribution to the Special Collection "Microporous materials: Crystal-chemistry, properties, and utilizations" – Associated Editors: G. Diego Gatta, Paolo Lotti)

Computer modeling of apparently straight bond angles: the intriguing case of all-silica ferrierite

Federica Trudu[a], Gloria Tabacchi[b], Ettore Fois[b]*

[a]SUPSI Lugano, Dipartimento Tecnologie Innovative, Via Cantonale 2c, Manno, CH-6928 Switzerland

[b]Dipartimento di Scienza e Alta Tecnologia, Università degli Studi dell'Insubria, and INSTM Insubria Research Unit, Via Valleggio 9, I-22100 Como, Italy.

Corrisponding author: Ettore Fois, ettore.fois@uninsubria.it

This is a preprint, the final version is subject to change, of the American Mineralogist (MSA)
Cite as Authors (Year) Title. American Mineralogist, in press.
DOI: https://doi.org/10.2138/am-2019-6951

ABSTRACT

The relationships between synthetic zeolites and their natural counterparts unveiled by theoretical studies have contributed to improve properties and applications of zeolite-based materials in strategic areas like industrial catalysis, environmental protection, and solar energy harvesting. To pinpoint the role of modeling in zeolite science, we discuss an example of computational-driven problem-solving: can tetrahedral frameworks sustain straight (i.e. 180°) Si-O-Si bond angles? The true crystal symmetry of zeolite ferrierite, especially in its all-silica form, has been intensely debated for 30 years before being solved in the *Pmnn* space group. Yet there are indications that an *Immm* structure with energetically unfavourable linear Si-O-Si linkages could be formed at high temperature. To gather insight, we perform density functional theory optimizations and frequency calculations of all-silica ferrierite in both the *Pmnn* and *Immm* space groups. Our results indicate that *Pmnn* is more stable than *Immm*, in line with experiments. While the *Pmnn* structure is a true minimum in the energy profile of ferrierite, the *Immm* structure has four imaginary frequency vibrations, three of which are localized on the 180° Si-O-Si angles. This suggest that ferrierites with *Immm* symmetry may be classified as metastable phases. Such a designation is also supported by first-principles molecular dynamics on *Immm* FER, evidencing that the average value of 180° actually results from Si-O-Si angle inversion. An implication of this study with interesting geological and technological consequences is the association of straight Si-O-Si angles experimentally detected in open-framework or low-density silicates to an angle-inversion process occurring at the femtosecond-scale. Such flexibility of the apparently flat Si-O-Si linkages might play an important role in sorption phenomena, which are ubiquitous in geological processes and industrial applications alike.

Keywords: Zeolites, Microporous materials, High temperature, framework flexibility, open framework silicates, molecular dynamics, density functional calculations

INTRODUCTION

Zeolites are porous silicates relevant in mineralogy, industry, and technology (Čejka et al. 2010; Gottardi and Galli 2012). Adsorption of geochemical fluids, solar energy transfer, or catalytic cracking all occur within zeolite nanospaces (Tabacchi 2018). These processes require multi-technique approaches in order to be understood, exploited, and improved (Van Speybroeck et al. 2015; Evans et al. 2017; Paul et al. 2018; Li and Pidko 2019). Computational techniques - such as geometric models (Sartbaeva et al. 2008; Wells and Sartbaeva 2012; Fletcher et al. 2015; Wells et al. 2015), force field methods (Demontis et al. 1991, 2017; Desbiens et al. 2005; Cailliez et al. 2008; Coudert et al. 2009; Demontis and Suffritti 2009; Wang et al. 2014) and quantum chemistry calculations (Campana et al. 1997; Ugliengo et al. 2005; Coudert et al. 2006; Giustetto et al. 2011; Dovesi et al. 2018) - are effective tools to address these issues.

Besides predicting crystal structures and elastic behaviour of geochemical systems (Kubicki 2016), simulations may guide experiments by providing atomistic insight often difficult to access in a laboratory (Marx and Hutter 2009; Tabacchi et al. 2014b; Van Speybroeck et al. 2015; Gaigeot and Sulpizi 2016). Theoretical techniques are particularly valuable at the temperature and pressure conditions typical of earth's mantle or extra-terrestrial environments (Cruciani 2006; Liang et al. 2007), where experimental observation is often unfeasible (Gatta et al. 2018; Kong et al. 2018). Zeolites are attractive materials for technology owing to their high resistance to thermal and mechanical stress (see (Lotti et al. 2016; Santoro et al. 2016; Comboni et al. 2018; Kim et al. 2018; Marqueño et al. 2018; Seryotkin and Bakakin 2018; Confalonieri et al. 2019; Gigli et al. 2019; Seryotkin 2019) for recent experimental studies and (Arletti et al. 2003; Cruciani 2006; Gatta 2008; Gatta and Lee 2014; Vezzalini

et al. 2014; Gatta et al. 2018) for reviews). Modeling, often combined with experiments, has enabled to analyze the deformation mechanisms of zeolites under high temperature/pressure conditions (Ballone et al. 2002; Ferro et al. 2002; White et al. 2004; Fois et al. 2008d; Jordá et al. 2013; Kremleva et al. 2013; Torres et al. 2013; Gatta et al. 2016; Bryukhanov et al. 2017; Demontis et al. 2017; Fischer 2018b). Insight from theory is also useful for zeolite-based applications, like hybrid functional materials (Calzaferri et al. 2003; Brühwiler et al. 2009; Fois et al. 2010b, 2012, 2013; Calzaferri 2012, 2017, 2018; Manzano et al. 2013; Zhou et al. 2013; Cucinotta et al. 2014; Viani et al. 2016; Insuwan et al. 2017; Li and Li 2018; Woodtli et al. 2018; Doungmanee et al. 2018; Pintus et al. 2019), or catalysts for pollutant abatement (Luo et al. 2016; Signorile et al. 2018; Wang et al. 2018a; Li and Pidko 2019; Prinsen and Luque 2019). For all these processes, the flexibility of the T-O-T angles (T is a tetrahedral cation, normally Si or Al) is crucial, and the framework often plays an active role (Fois et al. 2000; Spanó et al. 2006; Sirijaraensre and Limtrakul 2013; Montejo-Valencia and Curet-Arana 2015; Dong et al. 2016; Nie et al. 2017; Fang et al. 2018; Wang et al. 2018b). Many industrial catalysts have intriguing connections with mineralogy: for example, TS1 and natural mutinaite (Vezzalini et al. 1997) share the same MFI topology, and the ferrierite framework (FER) is common in the mineral world.

Natural FER is found both in volcanic and sedimentary rocks,(Yokomori et al. 2001) while hydrothermally synthesized ferrierites with high Si/Al ratio (Guo et al. 2000; Cheng et al. 2006) are excellent industrial catalysts (Corma 2003; de Ménorval et al. 2005; Bonilla et al. 2009). Moreover, all-silica ferrierite (Si-FER) is a very selective framework for bioethanol production (Bai et al. 2015): under high pressures, it acts as a mold, forming new supramolecular nanomaterials (Arletti et al. 2016, 2017a). Such peculiar behaviour suggests that compression might also enhance the yield of FER-catalyzed industrial processes (Wiedemann et al. 2016) by facilitating reactants' penetration in the pores. Also importantly, both adsorption (Bull et al. 1993) and catalytic power are influenced by the T-O-T angles (Redondo and Hay 1993; Buzzoni et al. 1996; Fois et al. 1998, 1999, 2008c; Tuma and

Sauer 2006; Trudu et al. 2007, 2008). Hence, understanding the structure-property relationships of Si-FER, the flexibility of the T-O-T linkages, and its symmetry becomes of key relevance in this context.

Overview of previous work

The true crystal symmetry of FER was subject of a debate lasting several decades. The structure refinement was first accomplished in space group *Immm* by Vaughan (Vaughan 1966). This highly symmetric group implies an inversion center at (0.25,0.25, 0.25), occupied by a bridging oxygen, and straight T-O-T linkages. This was in contrast with Liebau's proposition (Liebau 1961) that straight bonds are energetically unfavourable and should not exist in crystalline silicates at normal conditions. About 20 years later, several crystal structures were examined by Baur (Baur 1980), concluding that linear Si-O-Si bonds may occur in silicates and borosilicates (Baur and Ohta 1982). In 1985, Liebau pointed out that it is not possible to distinguish between dynamic and static disorder from diffraction experiments (Liebau 1985). While dynamic disorder refers to an atom vibrating about a time-averaged mean position, static disorder is related to an atom statistically occupying two (or more) positions close to a space-averaged mean position. Indeed, the high anisotropy of thermal vibrations of the oxygens involved in straight T-O-T bonds suggested that these atoms vibrate in a plane orthogonal to the T· · ·T direction. Shortly later, refinements of several FER crystal structures indicated that the inversion centers disappeared (Alberti 1986) and that the symmetry lowering was intrinsic to the framework (Alberti and Sabelli 1987b). The enigma of the FER symmetry captivated also Kuperman et al (Kuperman et al. 1993): using single-crystal X-ray diffraction, these authors concluded that the actual Si-FER symmetry was orthorhombic *Pmnn* and not *Immm*. By synchrotron X-ray and neutron powder diffraction, Morris et al highlighted significant distortions of Si-FER from the *Immm* symmetry (Morris et al. 1994). The bridging oxygen in the (assumed) linear T-O-T angle (namely, T1-O4-T1), was found 0.3 Å away from the ideal site, causing a reduction of the angle from 180° to about 170°. Although the

spread of the Si-O bond lengths (ca. 1.56-1.65 Å) was slightly larger than that found by the refinement in the 'incorrect' *Immm* group, a *Pmnn* symmetry for Si-FER was established. The same authors performed variable temperature NMR on a calcined sample of Si-FER (Bull et al. 2003), and hypothesised a temperature-induced transition at about 410 K from the *Pmnn* to the *Immm* form of the material. Albeit the researchers could not exclude that the high-temperature structure could be a dynamic average of the low temperature ones, as already suggested e.g., for quartz (Spearing et al. 1992), the data were in favour of *Immm* Si-FER at high temperature. However, the case of quartz suggests some considerations. Rigid-Unit-Mode (RUM) simulations on the quartz α-β transition showed that the highly-symmetric β-phase was a dynamic average: the instantaneous local structure exhibited large deviations from hexagonal symmetry due to cooperative tilting modes and was more similar to low-symmetry α-quartz (Wells et al. 2002; Sartbaeva et al. 2005). Similarly, the high-temperature cristobalite structure obtained from diffraction displayed a 180º Si–O–Si angle and large-amplitude motions of the oxygen normal to the Si-Si direction. Such dynamic disorder could be accounted for by low-frequency RUMs (Wells et al. 2002). Also, the influence of symmetry-breaking local-structure changes in zeolites was noted for analcime frameworks (Sartbaeva et al. 2008; Gatta et al. 2009; Wells et al. 2011): simulations suggested that the cubic symmetry resulted from a dynamic average over less symmetric structures (Gatta et al. 2009). Hence, various SiO_2-phases with linear Si-O-Si linkages are in fact of lower symmetry when viewed instantaneously and locally.

More recently, the high-pressure behaviour of Si-FER has been investigated on both powdered samples (Arletti et al. 2014) and single crystal (Lotti et al. 2015) using penetrating and non-penetrating fluids. Water intrusion in Si-FER was also studied at moderate pressures (Cailliez et al. 2008; Fraux et al. 2017). All these experiments indicated a *Pmnn* space group, thus ruling out the presence of 180° angles for Si-FER under compression. Nonetheless, it is worth mentioning that coesite – a high-pressure polymorph of silica– actually has Si-O-Si linkages of 180°, which remain linear even under GPa

pressures (Angel et al. 2003). Its structure (*C*/2*c* space group) is composed by four-membered rings of tetrahedra forming chains parallel to the *c* axis, and the Sil-Ol-Sil angle is symmetrically constrained to be 180° (Levien and Prewitt 1981). Differently from other silicates with supposed linear linkages (e.g. β-crystobalite), the displacement parameters for the O1 oxygen of coesite remained small in the explored pressure range – thus reflecting a limited degree of disorder. On this basis, Angel et al. concluded that the unusual 180° linkages were due to the connectivity of the coesite framework and not to its specific symmetry (Angel et al. 2003). This impressive stability was confirmed also by later studies: indeed, the Si1-O1-Si1 180° angle starts to bend only above ~ 20 GPa, leading to the appearance of two distinct angles, one of which remains however close to 180° (Černok et al. 2014; Chen et al. 2016). Hence, the case of coesite suggests that, in principle, we cannot exclude that the energetically unfavorable 180° angle in ferrierite (Morris et al. 1994; Lewis et al. 1996) might become a convenient arrangement under non-standard conditions (Bull et al. 2003).

Modeling may provide further insight on the true symmetry of ferrierite and the controversial existence of 180° angles in silicates. Most of the computational analyses performed to date adopted a *Pmnn* space group (Tuma and Sauer 2006; Fois et al. 2008b; Nachtigall et al. 2009; Grajciar et al. 2010; Fischer 2015; Fischer et al. 2015a, 2016; Hay et al. 2015; Fischer and Angel 2017), although some studies assumed an *Immm* symmetry (Coudert 2013; Román-Román and Zicovich-Wilson 2015). Herein, we consider FER models of *Immm* and *Pmnn* symmetry, optimize their structure, and compute harmonic frequencies to gather insight on their relative stability. Finally, the thermal behaviour of FER-*Immm* will be studied by first principles molecular dynamics.

METHODS

Adopted DFT functional and dispersion corrections

FER is a medium-sized type zeolite of the mordenite (MOR) family (Baerlocher et al. 2007). Its structure is based on five-membered rings of tetrahedra (5-MR) connected to form oval ten-ring channels (10-MR), both stacked along the [001] direction. Also present and running along the same direction is a smaller 6-MR channel. The 10-MR channels are intersected by eight-ring channels (8-MR), which run parallel to the [010] direction. Within the Density-Functional-Theory (DFT) framework, we have modelled the FER zeolite both in the *Immm* and *Pmnn* space groups using the PBE functional (Perdew et al. 1996) and dispersion corrections of the D2-type (Grimme 2006). This DFT functional/dispersion correction combination (nicknamed as PBE-D2), has been widely used in silicate modeling, providing a convenient accuracy/cost balance. Benchmark investigations (Fischer and Angel 2017) indicate even better performances for the (dispersion-corrected) PBE-sol functional in zero-K structural optimization of neutral zeotypes, although (dispersion-corrected) PBE seems to perform better for aluminophosphate zeotypes (Fischer 2018c). Nonetheless, those approaches deliver a rather similar description of bond distances and angles for zeolites and zeotypes. We chose PBE-D2 because, for the water-ethanol segregation in Si-FER (Arletti et al. 2017b, 2017a), it provided an average framework structure in good agreement with X-ray refinements, even at nonstandard conditions. PBE augmented with empirical dispersion has been employed to study various phenomena in porous materials, e.g. pressure-induced phase transitions (Kremleva et al. 2013, 2014), high-pressure template effects (Fischer 2018c), CO_2 adsorption (Fischer and Bell 2013b, 2013a, 2014), or zeolitic functional materials (Gigli et al. 2014, 2018a, 2018b; Tabacchi et al. 2015). The reliability of dispersion-corrected PBE has been demonstrated by extensive benchmark tests on solids (Tran et al. 2016), alumino-/germano-silicates (Fischer 2015, 2018a), aluminophosphates (Fischer 2019), silica polymorphs (Hay et al. 2015), and zeotypes (Fischer et al. 2015b, 2016, 2019; Fischer and Angel 2017; Albavera-Mata et al. 2018).

Generation of Si norm conserving pseudopotentials

Within the chosen protocol, the interactions of the electrons with the ionic cores are described by pseudopotentials, either of the ultrasoft (Vanderbilt 1990) or norm conserving (Kleinman and Bylander 1982; Troullier and Martins 1991) type (see below). Calculations were performed with CPMD (www.cpmd.org) and Quantum Espresso (QE) (Giannozzi et al. 2009, 2017). These codes were chosen because QE is effective in optimizing unit-cell parameters, while CPMD performs better in the first principles molecular dynamics (FPMD) runs (Car and Parrinello 1985; IBM Corp. 1990–2017 and MPI für Festkörperforschung Stuttgart 1997–2001 2017) . Although both codes describe the electronic structure with DFT using plane waves as basis sets, there are some relevant differences – e.g., QE also allows for the use of augmented plane waves and more flexible pseudopotential forms. This fact prompted us to use (in the case of O) or generate (in the case of Si) pseudopotentials able to work effectively with both codes and to provide equivalent results when tested on the same systems. The ultrasoft pseudopotential (PP) used for oxygen is the same for both codes and is available in the standard PP libraries of the QE distribution (www.quantum-espresso.org) and of the CPMD distribution (www.cpmd.org). The Si PPs we generated for the CPMD are of the norm-conserving type (Troullier and Martins 1991). Among these Si PPs, the three most promising candidates were tested (with both codes) on *Pmnn* FER and *Immm* FER against the original QE Si PP's (see Supporting information for details). The parameters of our best performing pseudopotential (named NCPP1) were obtained by fitting the Si pseudowavefunctions to the all-electron Si wavefunctions calculated for a Si atom in the s2p1d1 configuration. Notably, also the Si PP in the QE library had been generated by taking the Si s2p1d1 electronic configuration as reference state. In the case of *Pmnn* FER, structural results obtained with NCPP1 were validated against previous theoretical data obtained by (Fischer et al. 2016) with the same dispersion-corrected DFT functional (PBE-D2). The geometrical parameters monitored in these tests (i.e., bond lengths /angles) are reported in tables S1a to S4b in the Supporting Information. On the basis of these tests, NCPP1 was used in all the simulations with the CPMD code.

206 ***Computational setup***

207 The unit-cell parameter optimizations were carried out on *Immm* and *Pmnn* FER with QE, using the
208 ultrasoft PP's from the standard QE distribution and the experimental cell parameters and atomic
209 position from Ref. (Morris et al. 1994) as a guess. In these calculations, a 1x1x2 k-point mesh was
210 adopted. Electronic orbitals were expanded up to a kinetic energy cutoff of 60 Ry (833 eV) for the
211 wavefunction and 300 Ry (4998 eV) for the density), i.e. a value sufficient for convergence of the cell
212 parameters, in line with previous work on neutral zeotypes ((Hay et al. 2015; Fischer et al. 2016;
213 Albavera-Mata et al. 2018), aluminophosphates (Fischer and Angel 2017; Fischer 2018c) and other
214 framework materials (Formalik et al. 2018). Such a step gave us the fully optimized minimum energy
215 structures for FER *Immm* and FER *Pmnn* at zero K, which we used as a reference for the other
216 calculations. The optimized lattice parameters are reported in Table 1.

217 Calculations with the CPMD code were performed taking the parameters in Table 1 and doubling the
218 cell parameter *c*. The CPMD simulation cell contains 216 atoms (stoichiometry: $Si_{72}O_{144}$). The larger
219 size of the CPMD cell with respect to the QE cell allows for considering only the Gamma Point in the
220 Brillouin zone sampling. The CPMD minimum energy structure is well in line with the QE one
221 obtained with a similar setup (see Tables 1-4a,b,c,d in the Supporting information). As frequency
222 calculations require a strict convergence criterion (Marx and Hutter 2009), we considered convergence
223 achieved when the maximum forces on the ions were lower than 5×10^{-5} Hartree/Bohr. Using the
224 CPMD optimized geometry at 60 Ry cutoff, harmonic frequencies and eigenvectors were calculated
225 with a finite difference method and the same set-up as in the optimization runs. Relevant normal modes
226 were analysed by plotting the atomic displacements as vectors centered on the atomic positions. The
227 optimized geometries at 60 Ry cutoff were then re-optimized for lower cutoff values (30 Ry for
228 wavefunction, 240 Ry for the density; 25 Ry for wavefunction, 200 Ry for density) to check whether

229 convergence of geometric parameters could be achieved in a computationally-cheaper way – which is
230 crucial for long FPMD runs. As such tests gave positive results, the lower plane wave cutoffs (25 Ry
231 for wavefunction, 200 Ry for density) were used in the FPMD simulations on FER *Immm*. FPMDs
232 were performed with the Car-Parrinello (CP) method (Car and Parrinello 1985) in the NVE ensemble.
233 First, we performed a 10 ps equilibration run in the NVT ensemble at a target temperature of 450K
234 with Nose-Hoover thermostats (Nosé 1984; Hoover 1985). Such a target value was chosen because, as
235 reported by Ref. (Bull et al. 2003), for T> 400 K the *Immm* structure should become favored over the
236 *Pmnn* one. After equilibration, the trajectory was followed for 50 ps to calculate the average
237 coordinates of *Immm* Si-FER. The average temperature resulted 438 K (with 17 K standard deviation).
238 The equations of motion from the CP Lagrangean were integrated with a time step of 5 au and an
239 inertia parameter for the wavefunction coefficients of 500 au. Such FPMD parameters properly
240 described the dynamics of zeolite hybrids (Fois et al. 2010b, 2012; Zhou et al. 2013), the high-pressure
241 behaviour of zeolites (Ferro et al. 2002; Ceriani et al. 2004; Fois et al. 2005, 2008d; Betti et al. 2007;
242 Gatta et al. 2016; Fois and Tabacchi 2019) and high-temperature processes of oxide porous materials
243 and interfaces (Fois et al. 2003, 2008a, 2010a; Tabacchi et al. 2014a, 2016a, 2007; Barreca et al. 2011,
244 2018; Deiana et al. 2013, 2016; Martínez-Suarez et al. 2015; Kraus and Frank 2017). Apart from the
245 cell parameters (that were kept fixed along the simulation), no constraints were imposed to the atomic
246 positions, i.e. all atoms were left free to evolve according to the equations of motions, thus the
247 symmetry of the system was fully unconstrained. Graphical representations of the FER structures were
248 created with the VMD code (Humphrey et al. 1996), https://www.ks.uiuc.edu/.

249

250 **RESULTS AND DISCUSSION**

The optimized cell parameters of ferrierite are reported in Table 1. By considering that the cell parameters (and the atomic coordinates) from DFT-structural optimizations refer to minimum structures at 0 K, while experimental structural data are clearly obtained from finite temperature measurements, the cell parameters calculated for *Pmnn* Si-FER are in keeping with the corresponding experimental ones (Morris et al. 1994; Lewis et al. 1996). Moreover, our Si-FER *Pmnn* cell parameters are also in line with the results of previous theoretical studies (Hay et al. 2015; Fischer et al. 2016; Fischer and Angel 2017), including those obtained by (Fischer et al. 2016) using the same combination of density functional/dispersion correction and a comparable energy cutoff (800 eV). It is worth underlining that several dispersion-corrected versions of widely-used density functionals provide a satisfactory performance for structural parameters of zeolites, as shown e.g. in Ref. (Fischer 2015, 2018c; Fischer et al. 2016; Fischer and Angel 2017).

The cell parameters obtained for *Immm* (Table 1) favourably compare with those reported for the FER-*Immm* framework in the IZA-SC database of Zeolite Structures (Baerlocher et al. 2007; Baerlocher and McCusker 2017). Noticeably, the calculated *Immm* parameters are all slightly longer than the *Pmnn* ones, resulting thus into a larger cell volume than Si-FER *Pmnn*, also in line with experimental data. The Si-O bond distances and Si-O-Si bond angles calculated for the *Pmnn* and *Immm* structures of Si-FER are reported in the supporting information (Tables 1a-d and Tables 2a-d, respectively); since the *Immm* and *Pmnn* space groups bear a different number of crystallographically different atoms in the unit cell, it is not possible to describe the two structures with a single labelling scheme. More importantly, the comparison of the calculated *Pmnn* and *Immm* minimum energy structures indicates that the former one is the most stable phase at 0 K – specifically, the energy difference per formula unit amounts to 0.15 kcal/mol in favour of *Pmnn*. This finding is in line with the now generally accepted space group of Si-FER, *Pmnn*, supported by the broad series of experimental and theoretical results discussed in the introduction. Moreover, a clear distinction between the *Pmnn* and *Immm* structures of

ferrierite emerges from the vibrational analysis of the calculated energy minima. All the vibrational frequencies of *Pmnn* are positive, which indicates that this structure is a stable minimum of the potential energy surface of FER. This result provides further support to the *Pmnn* space group assignment for Si-FER. In contrast, four frequencies calculated for *Immm* are imaginary, indicating that this structure is not a stable minimum of the potential energy surface of Si-FER. This important finding suggests a closer analysis of the four normal modes corresponding to the imaginary frequencies. The graphical representations of these modes, labelled Mode1 to Mode4, are displayed in Figures 4 to 7 in the Supporting Information, respectively. Since these modes involve neither stretching of Si-O bonds nor bending of O-Si-O angles, but only tilting of tetrahedra, they may be assimilated to rigid unit modes (Swainson and Dove 1993; Matthew et al. 2001; Wells et al. 2002; Sartbaeva et al. 2005). First, we observe that not all the modes imply variation of the Si1-O4-Si1 angle. In particular, Mode1 takes place in the *bc* plane: it may be described as a collective zig-zag corrugation of the tetrahedral chains along the *c* direction, is localized on the Si1-O2-Si2, Si1-O1-Si3, Si3-O7-Si4, Si3-O8-Si4 linkages, and exhibits a *C2/m* symmetry. The other three modes show significant contributions from the Si1-O4-Si1 linkages and cause distortions of the bond angle from the 180º value during vibration. Moreover, the displacement of the O4 atoms is always more pronounced than those of the Si1 atoms, in line with the flexibility behaviour expected for tetrahedral T-O-T linkages. Interestingly, in Mode2 the motion of the O4 atom occurs in the *ab* plane of *Immm*-FER, while in Mode3 and Mode4 the O4 displacement is in the *ac* and *bc* planes, respectively. Anyway, in all three modes the O4 atoms move nearly perpendicular to the Si1----S1 axis, i.e. according to the dynamical disorder mechanisms previously postulated for Si-FER (Liebau 1985; Alberti 1986; Alberti and Sabelli 1987a) and discussed in the Introduction. In addition to the Si-O4-Si1 linkage, these modes involve other atoms of the Si-FER framework. Mode2 has a significant participation of the Si1-O2-Si2 linkages, plus a minor contribution of the Si1-O1-Si3 ones, resulting thus into a breathing deformation of the 10MR in the *ab* plane. The Si3-O7-Si4 and Si3-

O8-Si4 bonds of the 5MR containing the Si-O4-Si1 linkages are involved as well, yet to a minor extent. Mode4 essentially involve the same linkages as in Mode2, but now they contribute nearly equally to the mode, and the O4 displacements occur mostly in the ac plane. Mode3 also involves Si1-O3-Si1 and Si2-O2-Si2, and brings about a collective deformation of the 8MR. The atomic displacement analysis of the three angle-changing modes indicates that Mode2 and Mode4 belong to *I2mm*, while Mode3 to *Imm2*. Indeed both *I2mm* and *Imm2* are orthorhombic (space group 44), and can be obtained from *Immm* by removing the inversion center on the O4 positions. In contrast, Mode1 does not change the S1-O4-Si1 angle and has a much lower symmetry, as it belongs to the monoclinic *C2/m* (12).

To demonstrate that *Immm*-FER spontaneously evolves to lower-symmetry structures, starting from the *Immm* optimized structure we displaced all atomic coordinates along the normal mode eigenvectors associated to the imaginary frequencies, and reoptimized the geometry without symmetry constraints. Indeed, the four resulting optimized geometries, which maintained the symmetry of the respective modes, were all lower in energy than Si-FER *Immm* (see Table 2). Although the structure optimized from Mode1 keeps the 180° angle, its symmetry (monoclinic *C2/m*) is lower than the orthorhombic *Pmnn* symmetry of Si-FER at normal conditions. In contrast, the three orthorhombic structures are all characterized by angles different from 180° - i.e., 165.4°, 166,1 and 172.2°, respectively. Yet all the four structures have higher energy compared to Si-FER *Pmnn* – which is therefore the most stable form and true minimum of Si-FER. Thus, the *Immm* structure should not be regarded as a stable configuration, but rather as a negative-curvature region of the potential energy surface of Si-FER leading to more stable symmetry-breaking forms. Such metastability appears to be a feature common to other highly symmetric silicates, which have several flexible modes able to break the symmetry of the structure (Wells et al. 2002; Gatta et al. 2009).

Our analysis seem to prove the instability of straight Si-O-Si angles in ferrierite - in line with Liebau's proposition that 180° angles in aluminosilicates are energetically unfavored (Liebau 1961), and hence to exclude stable *Immm* phases of Si-FER. On the other hand, such structure has been proposed to form at high temperature on the basis of in-situ MAS-NMR and single crystal X-ray diffraction measurements (Bull et al. 2003).

We show that such a contradiction is only apparent because the key variable of the process – temperature - has not been accounted for yet. Hence, we "heated" the *Immm* simulation system up to 450 K, let it equilibrate and followed its time evolution for about 50 ps. Figure 3 clearly shows that the average atomic positions obtained from the simulations correspond to a *Immm* Si-FER structure and exhibit Si1-O4-Si1 angles of 180°, in line with the structural data emerging from the high-temperature experiments of Ref. (Bull et al. 2003). Nevertheless, the instantaneous positions of the individual Si1, O4, and Si1 atoms sampled along the trajectory indicate that the inversion of the Si1-O4-Si1 angle occurs regularly and continuously on the femtosecond time scale. More specifically, the atomic positions are symmetrically distributed along the line corresponding to the 180° angle, and the resulting 180° value is due to dynamical disorder induced by temperature. Remarkably, this result can be easily rationalized by considering that the energy difference that at standard conditions favours the *Pmnn* (~ 0.15 kcal/mol) is largely overcome by the thermal energy, that amounts to ~ 0.8 kcal/mol at 400 K.

Overall, our data suggest that the *Immm* structure of high-temperature Si-FER (Bull et al. 2003) should rather be viewed as a result of dynamic averaging over configurations exhibiting a lower symmetry. This interpretation is in line with previous propositions for high-symmetry, high-temperature silicate phases, such as β-quartz and cubic analcime based on RUM calculations (Wells et al. 2002; Gatta et al. 2009), and points out the essential role of the flexibility of the zeolite framework. Indeed although the Si1-O4-Si1 linkage could be found instantaneously in the linear arrangement, such a configuration is

344 energetically disfavoured: hence, these atoms vibrate around their equilibrium positions to allow the O4
345 bridging oxygen to continuously change its positioning with respect to the Si1----Si1 line, so as to
346 avoid as much as possible the formation of the 180° angle. The consequence of this behavior is the
347 angle inversion mechanism highlighted for high-temperature Si-FER. Interestingly, an analogous
348 behaviour has been recently predicted by DFT calculations for template-containing CHA-
349 aluminophosphates under high compression (Fischer 2018c). Specifically, the pressure-induced
350 inversion of one of the equatorial Al-O-P linkages of the *d6r* building unit, accompanied by a
351 considerable deformation of these units, has been associated to the presence of AlO_4F_2 octahedra, and
352 has been shown to depend on the nature of the organic template occupying the CHA cage (Fischer
353 2018c). Hence, these examples indicate that the inherent flexibility of apparently linear T-O-T linkages
354 appear to be a more general aspect of the behavior of crystalline framework silicates, aluminosilicates
355 or aluminophosphates when subjected to high pressure or high temperature conditions. Actually the
356 case of coesite is somewhat different: dynamical disorder appears only at very high temperatures
357 (above 1300 K) (Bourova et al. 2004; Bourova and Petitet 2006), and, at room temperature, the straight
358 Si-O-Si linkages persist up to ~ 20 GPa. This stiffness appears to be a direct consequence of the
359 extremely compact packing of SiO_4 tetrahedra in coesite, which hinders the variation of Si–O–Si angles
360 with increasing temperatures and pressures (Richet and Ottonello 2014). On the contrary, in open-
361 framework structures like Si-FER, the inherent flexibility of the linkages allows to achieve Si-O-Si
362 angle inversion at a low energetic cost.

363 **IMPLICATIONS**

364 We showed that the high temperature structure of Si- FER has on average an *Immm* symmetry and
365 angles of 180 degrees. Yet, when viewed instantaneously, its true symmetry is lower, and inversions of
366 the angle actually occur at the femtosecond timescale.

Interestingly, the insight obtained from the application of DFT techniques to the ferrierite case corroborates a behaviour observed by other experimental and modelling methods in analogous systems, namely that highly symmetric phases like cubic analcime (Gatta et al. 2009) and beta-quartz (Wells et al. 2002; Sartbaeva et al. 2005) should be considered as dynamic averages over lower-symmetry structures. An angle-inversion mechanism has been predicted by DFT simulations also for some aluminophosphates under high-pressure (Fischer 2018c). In a different way, the existence of truly linear Si-O-Si linkages could not be excluded in coesite, in view of the low disorder found for the bridging oxygen positions, consequence of the higher density of this phase (Angel et al. 2003). Indeed, an intriguing value of 180º has also been recently proposed for a high-pressure form of phosphorous oxonitride with coesite crystal structure (Baumann et al. 2015).

Our results bear profound geological implications. The strict relationship between flat Si-O-Si angles and metastability of a zeolite framework might represent a key to better understand the possible phase-transition mechanisms of open-framework (alumino-) silicate minerals (e.g., zeolites, feldspathoids, feldspars) under non-standard, non-ambient conditions, which typically coincide with the elevated pressures and temperatures of geological relevance. For example, the deviation from a Si-O-Al angle of 180° causes the spectacular *P*-induced iso-symmetric first-order phase transition in kalsilite ($KAlSiO_4$) at 3.5 GPa, as reported by Gatta et al. (2011)(Gatta et al. 2011), with a drastic change of the mineral density and of the deformation mechanisms at atomic scale, coupled with a completely different anisotropic compressional scheme for the two polymorphs. Similarly, the *P*-induced deviation from a Si-O-Al angle of 180° in davyne at high pressure makes the structure unstable already at very low *P* and drives a $P6_3/m$-to-$P6_3$ displacive phase transition at ~ 0.38 GPa (Lotti et al. 2014). These two examples show how the configuration of the T-O-T angle equal to 180° or different from that value can have a drastic impact on the structure stability of open-framework silicates.

In a broader perspective, the Si-O-Si angle inversion mechanism may help to achieve a deeper general knowledge of sorption/desorption events in zeolites. These processes essentially involve molecules – which may enter, remain outside, or leave the pores according not only to trivial relative size considerations, but also thanks to the flexibility of both molecular species and host framework. Such flexibility may help rationalize various technologically important phenomena in zeolites, such as catalytic performances of Lewis-acid sites (Luo et al. 2016), window effects (Balestra et al. 2015; Coudert and Kohen 2017; Ke et al. 2019), fabrication of functional materials (Tabacchi et al. 2015, 2016b) or hybrid nanocatalysts (Zendehdel et al. 2018). All these phenomena essentially involve correlated vibrational motions of guest molecules and zeolite framework, and collective oscillations of the T-O-T bond angles.

ACKNOWLEDGEMENTS

This work was supported by the Italian MIUR, within the frame of the following projects: PRIN2015 "ZAPPING" High-pressure nano-confinement in Zeolites: the Mineral Science know-how APPlied to engineerING of innovative materials for technological and environmental applications (2015HK93L7), ImPACT (FIRB RBFR12CLQD), and University of Insubria Far 2017. We gratefully acknowledge the Reviewers of this manuscript for their insightful comments.

DEDICATION

We dedicate this manuscript to the memory of the late Prof. Alberto Alberti.

REFERENCES

Albavera-Mata, A., Zicovich-Wilson, C.M., Gázquez, J.L., Trickey, S.B., and Vela, A. (2018) Long-

411 range exchange limit and dispersion in pure silica zeolites. Theoretical Chemistry Accounts, 137,
412 26.

413 Alberti, A. (1986) The absence of T-O-T angles of 180° in zeolites. In Studies in Surface Science and
414 Catalysis Vol. 28, pp. 437–441. Elsevier.

415 Alberti, A., and Sabelli, C. (1987a) Statistical and true symmetry of ferrierite: Possible absence of
416 straight T-T bridging bonds. Zeitschrift fur Kristallographie - New Crystal Structures, 178, 249–
417 256.

418 ——— (1987b) Statistical and true symmetry of ferrierite: possible absence of straight T—O—T
419 bridging bonds. Zeitschrift für Kristallographie - Crystalline Materials, 178, 249–256.

420 Angel, R.J., Shaw, C.S.J., and Gibbs, G. V. (2003) Compression mechanisms of coesite. Physics and
421 Chemistry of Minerals, 30, 167–176.

422 Arletti, R., Ferro, O., Quartieri, S., Sani, A., Tabacchi, G., and Vezzalini, G. (2003) Structural
423 deformation mechanisms of zeolites under pressure. American Mineralogist, 88, 1416–1422.

424 Arletti, R., Vezzalini, G., Quartieri, S., Di Renzo, F., and Dmitriev, V. (2014) Pressure-induced water
425 intrusion in FER-type zeolites and the influence of extraframework species on structural
426 deformations. Microporous and Mesoporous Materials, 191, 27–37.

427 Arletti, R., Ronchi, L., Quartieri, S., Vezzalini, G., Ryzhikov, A., Nouali, H., Daou, T.J., and Patarin, J.
428 (2016) Intrusion-extrusion experiments of MgCl2 aqueous solution in pure silica ferrierite:
429 Evidence of the nature of intruded liquid by in situ high pressure synchrotron X-ray powder
430 diffraction. Microporous and Mesoporous Materials, 235, 253–260.

431 Arletti, R., Fois, E., Gigli, L., Vezzalini, G., Quartieri, S., and Tabacchi, G. (2017a) Irreversible

Conversion of a Water–Ethanol Solution into an Organized Two-Dimensional Network of Alternating Supramolecular Units in a Hydrophobic Zeolite under Pressure. Angewandte Chemie - International Edition, 56, 2105–2109.

Arletti, R., Fois, E., Tabacchi, G., Quartieri, S., and Vezzalini, G. (2017b) Pressure-Induced Penetration of Water-Ethanol Mixtures in All-Silica Ferrierite. Advanced Science Letters, 23, 5966–5969.

Baerlocher, C., and McCusker, L.B. (2017) Database of Zeolite Structures http://www.iza-structure.org/databases/. International Zeolite Association.

Baerlocher, C., McCusker, L.B., and Olson, D.H. (2007) Atlas of Zeolite framework types, 398 p. Published on behalf of the Structure Commission of the International Zeolite Association by Elsevier.

Bai, P., Jeon, M.Y., Ren, L., Knight, C., Deem, M.W., Tsapatsis, M., and Siepmann, J.I. (2015) Discovery of optimal zeolites for challenging separations and chemical transformations using predictive materials modeling. Nat Commun, 6.

Balestra, S.R.G., Hamad, S., Ruiz-Salvador, A.R., Domínguez−García, V., Merkling, P.J., Dubbeldam, D., and Calero, S. (2015) Understanding Nanopore Window Distortions in the Reversible Molecular Valve Zeolite RHO. Chemistry of Materials, 27, 5657–5667.

Ballone, P., Quartieri, S., Sani, A., and Vezzalini, G. (2002) High-pressure deformation mechanism in scolecite: A combined computational-experimental study. American Mineralogist, 87, 1194–1206.

Barreca, D., Fois, E., Gasparotto, A., Seraglia, R., Tondello, E., and Tabacchi, G. (2011) How does CuII convert into CuI? An unexpected ring-mediated single-electron reduction. Chemistry - A

453 European Journal, 17, 10864–10870.

454 Barreca, D., Carraro, G., Fois, E., Gasparotto, A., Gri, F., Seraglia, R., Wilken, M., Venzo, A., Devi,
455 A., Tabacchi, G., and others (2018) Manganese(II) Molecular Sources for Plasma-Assisted CVD
456 of Mn Oxides and Fluorides: From Precursors to Growth Process. The Journal of Physical
457 Chemistry C, 122, 1367–1375.

458 Baumann, D., Niklaus, R., and Schnick, W. (2015) A High-Pressure Polymorph of Phosphorus
459 Oxonitride with the Coesite Structure. Angewandte Chemie International Edition, 54, 4388–4391.

460 Baur, W. (1980) Straight Si-O-Si bridging bonds do exist in silicates and silicon dioxide polymorphs.
461 Acta Crystallographica Section B, 36, 2198–2202.

462 Baur, W.H., and Ohta, T. (1982) The Si5O16 pentamer in zunyite refined and empirical relations for
463 individual silicon-oxygen bonds. Acta Crystallographa, B38, 390–401.

464 Betti, C., Fois, E., Mazzucato, E., Medici, C., Quartieri, S., Tabacchi, G., Vezzalini, G., and Dmitriev,
465 V. (2007) Gismondine under HP: Deformation mechanism and re-organization of the extra-
466 framework species. Microporous and Mesoporous Materials, 103, 190–209.

467 Bonilla, A., Baudouin, D., and Pérez-Ramírez, J. (2009) Desilication of ferrierite zeolite for porosity
468 generation and improved effectiveness in polyethylene pyrolysis. Journal of Catalysis, 265, 170–
469 180.

470 Bourova, E., and Petitet, J.-P. (2006) Coesite (SiO2) as an extreme case of superheated crystal: An X-
471 ray diffraction study up to 1776 K. Chemical Geology, 229, 57–63.

472 Bourova, E., Parker, S.C., and Richet, P. (2004) High-temperature structure and dynamics of coesite
473 (SiO2) from numerical simulations. Physics and Chemistry of Minerals, 31, 569–579.

Brühwiler, D., Calzaferri, G., Torres, T., Ramm, J.H., Gartmann, N., Dieu, L.-Q., López-Duarte, I., and Martínez-Díaz, M.V. (2009) Nanochannels for supramolecular organization of luminescent guests. Journal of Materials Chemistry, 19, 8040–8067.

Bryukhanov, I.A., Rybakov, A.A., Larin, A. V, Trubnikov, D.N., and Vercauteren, D.P. (2017) The role of water in the elastic properties of aluminosilicate zeolites: DFT investigation. Journal of Molecular Modeling, 23, 68.

Bull, I., Lightfoot, P., Villaescusa, L.A., Bull, L.M., Gover, R.K.B., Evans, J.S.O., and Morris, R.E. (2003) An X-ray diffraction and MAS NMR study of the thermal expansion properties of calcined siliceous ferrierite. Journal of the American Chemical Society, 125, 4342–4349.

Bull, L.M., Henson, N.J., Cheetham, A.K., Newsam, J.M., and Heyes, S.J. (1993) Behavior of benzene in siliceous faujasite: a comparative study of deuteron NMR and molecular dynamics. The Journal of Physical Chemistry, 97, 11776–11780.

Buzzoni, R., Bordiga, S., Ricchiardi, G., Lamberti, C., Zecchina, A., and Bellussi (1996) Interaction of Pyridine with Acidic (H-ZSM5, H-β, H-MORD Zeolites) and Superacidic (H-Nafion Membrane) Systems: An IR Investigation. Langmuir, 12, 930–940.

Cailliez, F., Trzpit, M., Soulard, M., Demachy, I., Boutin, A., Patarin, J., and Fuchs, A.H. (2008) Thermodynamics of water intrusion in nanoporous hydrophobic solids. Physical Chemistry Chemical Physics, 10, 4817.

Calzaferri, G. (2012) Nanochannels: Hosts for the supramolecular organization of molecules and complexes. Langmuir, 28, 6216–6231.

——— (2017) Entropy in multiple equilibria, theory and applications. Phys. Chem. Chem. Phys., 19,

10611–10621.

——— (2018) Entropy in multiple equilibria, compounds with different sites. Physical Chemistry Chemical Physics, 20, 29070–29084.

Calzaferri, G., Huber, S., Maas, H., and Minkowski, C. (2003) Host-guest antenna materials. Angewandte Chemie - International Edition, 42, 3732–3758.

Campana, L., Selloni, A., Weber, J., and Goursot, A. (1997) Cation siting and dynamical properties of zeolite offretite from first-principles molecular dynamics. Journal of Physical Chemistry B, 101, 9932–9939.

Car, R., and Parrinello, M. (1985) Unified Approach for Molecular Dynamics and Density-Functional Theory. Physical Review Letters, 55, 2471–2474.

Čejka, J., Corma, A., and Zones, S. (2010) Zeolites and catalysis: synthesis, reactions and applications, Volume 2, 881 p. (J. Čejka, A. Corma, & S. Zones, Eds.). WILEY-VCH Verlag GmbH & Co. KGaA, Weinheim, Germany.

Ceriani, C., Fois, E., Gamba, A., Tabacchi, G., Ferro, O., Quartieri, S., and Vezzalini, G. (2004) Dehydration dynamics of bikitaite: Part II. Ab initio molecular dynamics study. American Mineralogist, 89, 102–109.

Černok, A., Bykova, E., Ballaran, T.B., Liermann, H.-P., Hanfland, M., and Dubrovinsky, L. (2014) High-pressure crystal chemistry of coesite-I and its transition to coesite-II. Zeitschrift für Kristallographie - Crystalline Materials, 229, 761–773.

Chen, T., Wang, X., Qi, X., Ma, M., Xu, Z., and Li, B. (2016) Elasticity and phase transformation at high pressure in coesite from experiments and first-principles calculations. American

516 Mineralogist, 101, 1190–1196.

517 Cheng, X., Wang, J., Guo, J., Sun, J., and Long, Y. (2006) High-Silica Ferrierite Zeolite Self-
518 Transformed from Aluminosilicate Gel. ChemPhysChem, 7, 1198–1202.

519 Comboni, D., Gatta, G.D., Lotti, P., Merlini, M., and Hanfland, M. (2018) Crystal-fluid interactions in
520 laumontite. Microporous and Mesoporous Materials, 263, 86–95.

521 Confalonieri, G., Quartieri, S., Vezzalini, G., Tabacchi, G., Fois, E., Daou, T.J., and Arletti, R. (2019)
522 Differential penetration of ethanol and water in Si-chabazite: High pressure dehydration of
523 azeotrope solution. Microporous and Mesoporous Materials, 284, 161–169.

524 Corma, A. (2003) State of the art and future challenges of zeolites as catalysts. Journal of Catalysis,
525 216, 298–312.

526 Coudert, F.-X., and Kohen, D. (2017) Molecular Insight into CO_2 "Trapdoor" Adsorption in Zeolite
527 Na-RHO. Chemistry of Materials, 29, 2724–2730.

528 Coudert, F.-X., Vuilleumier, R., and Boutin, A. (2006) Dipole Moment, Hydrogen Bonding and IR
529 Spectrum of Confined Water. ChemPhysChem, 7, 2464–2467.

530 Coudert, F.-X., Cailliez, F., Vuilleumier, R., Fuchs, A.H., and Boutin, A. (2009) Water nanodroplets
531 confined in zeolite pores. Faraday Discuss., 141, 377–398.

532 Coudert, F.X. (2013) Systematic investigation of the mechanical properties of pure silica zeolites:
533 Stiffness, anisotropy, and negative linear compressibility. Physical Chemistry Chemical Physics,
534 15, 16012–16018.

535 Cruciani, G. (2006) Zeolites upon heating: Factors governing their thermal stability and structural
536 changes. Journal of Physics and Chemistry of Solids, 67, 1973–1994.

Cucinotta, F., Guenet, A., Bizzarri, C., Mroz, W., Botta, C., Milian-Medina, B., Gierschner, J., and De Cola, L. (2014) Energy transfer at the zeolite l boundaries: Towards photo- and electroresponsive materials. ChemPlusChem, 79, 45–57.

de Ménorval, B., Ayrault, P., Gnep, N.S., and Guisnet, M. (2005) Mechanism of n-butene skeletal isomerization over HFER zeolites: a new proposal. Journal of Catalysis, 230, 38–51.

Deiana, C., Tabacchi, G., Maurino, V., Coluccia, S., Martra, G., and Fois, E. (2013) Surface features of TiO2 nanoparticles: Combination modes of adsorbed CO probe the stepping of (101) facets. Physical Chemistry Chemical Physics, 15, 13391–13399.

Deiana, C., Fois, E., Martra, G., Narbey, S., Pellegrino, F., and Tabacchi, G. (2016) On the Simple Complexity of Carbon Monoxide on Oxide Surfaces: Facet-Specific Donation and Backdonation Effects Revealed on TiO2 Anatase Nanoparticles. ChemPhysChem, 17, 1956–1960.

Demontis, P., and Suffritti, G.B. (2009) A comment on the flexibility of framework in molecular dynamics simulations of zeolites. Microporous and Mesoporous Materials, 125, 160–168.

Demontis, P., Suffritti, G.B., Quartieri, S., Gamba, A., and Fois, E.S. (1991) Molecular dynamics studies on zeolites. Part 5. - Discussion of the structural changes of silicalite. Journal of the Chemical Society, Faraday Transactions, 87, 1657–1663.

Demontis, P., Gulín-González, J., Ruiz-Puentes, A., Sant, M., Gabrieli, A., and Suffritti, G.B. (2017) Computational Studies on the Effects of Pressure and Temperature on Zeolite Framework Structures. Advanced Science Letters, 23, 5824–5827.

Desbiens, N., Demachy, I., Fuchs, A.H., Kirsch-Rodeschini, H., Soulard, M., and Patarin, J. (2005) Water condensation in hydrophobic nanopores. Angewandte Chemie - International Edition, 44,

558 5310–5313.

559 Dong, J., Zhu, H., Xiang, Y., Wang, Y., An, P., Gong, Y., Liang, Y., Qiu, L., Zheng, A., Peng, X., and
560 others (2016) Toward a Unified Identification of Ti Location in the MFI Framework of High-Ti-
561 Loaded TS-1: Combined EXAFS, XANES, and DFT Study. The Journal of Physical Chemistry C,
562 120, 20114–20124.

563 Doungmanee, S., Siritanon, T., Insuwan, W., Jungsuttiwong, S., and Rangsriwatananon, K. (2018)
564 Multi step energy transfer between three Si_LTL and SiGe_LTL zeolite-loaded dyes. Journal of
565 Porous Materials, 25, 1381–1389.

566 Dovesi, R., Erba, A., Orlando, R., Zicovich-Wilson, C.M., Civalleri, B., Maschio, L., Rérat, M.,
567 Casassa, S., Baima, J., Salustro, S., and others (2018) Quantum-mechanical condensed matter
568 simulations with CRYSTAL. Wiley Interdisciplinary Reviews: Computational Molecular Science,
569 8, e1360.

570 Evans, J.D., Fraux, G., Gaillac, R., Kohen, D., Trousselet, F., Vanson, J.-M., and Coudert, F.-X. (2017)
571 Computational Chemistry Methods for Nanoporous Materials. Chemistry of Materials, 29, 199–
572 212.

573 Fang, X., Wu, L., Yu, Y., Sun, L., and Liu, Y. (2018) Improving the catalytic performance of TS-1
574 through Zn(AC)2modification. Catalysis Communications, 114, 1–5.

575 Ferro, O., Quartieri, S., Vezzalini, G., Fois, E., Gamba, A., and Tabacchi, G. (2002) High-pressure
576 behavior of bikitaite: An integrated theoretical and experimental approach. American
577 Mineralogist, 87, 1415–1425.

578 Fischer, M. (2015) Structure and bonding of water molecules in zeolite hosts: Benchmarking plane-

wave DFT against crystal structure data. Zeitschrift für Kristallographie - Crystalline Materials, 230, 325–336.

——— (2018a) Local Environment and Dynamic Behavior of Fluoride Anions in Silicogermanate Zeolites: A Computational Study of the AST Framework. The Journal of Physical Chemistry C, acs.jpcc.8b10770.

——— (2018b) Porous aluminophosphates as adsorbents for the separation of CO 2 /CH 4 and CH 4 /N 2 mixtures – a Monte Carlo simulation study. Sustainable Energy & Fuels, 2, 1749–1763.

——— (2018c) Template effects on the pressure-dependent behavior of chabazite-type fluoroaluminophosphates: A computational approach. Physics and Chemistry of Minerals, 1–17.

——— (2019) First-Principles Study of AlPO4-H3, a Hydrated Aluminophosphate Zeotype Containing Two Different Types of Adsorbed Water Molecules. Molecules, 24, 922.

Fischer, M., and Angel, R.J. (2017) Accurate structures and energetics of neutral-framework zeotypes from dispersion-corrected DFT calculations. The Journal of Chemical Physics, 146, 174111.

Fischer, M., and Bell, R.G. (2013a) A dispersion-corrected density-functional theory study of small molecules adsorbed in alkali-exchanged chabazites. Zeitschrift für Kristallographie - Crystalline Materials, 228, 124–133.

——— (2013b) Modeling CO_2 Adsorption in Zeolites Using DFT-Derived Charges: Comparing System-Specific and Generic Models. The Journal of Physical Chemistry C, 117, 24446–24454.

——— (2014) Interaction of hydrogen and carbon dioxide with sod-type zeolitic imidazolate frameworks: a periodic DFT-D study. CrystEngComm, 16, 1934.

Fischer, M., Delgado, M.R., Areán, C.O., and Duran, C.O. (2015a) CO adsorption complexes in

zeolites: How does the inclusion of dispersion interactions affect predictions made from DFT calculations? The case of Na-CHA. Theoretical Chemistry Accounts, 134, 91.

——— (2015b) CO adsorption complexes in zeolites: How does the inclusion of dispersion interactions affect predictions made from DFT calculations? The case of Na-CHA. Theoretical Chemistry Accounts, 134, 91.

Fischer, M., Evers, F.O., Formalik, F., and Olejniczak, A. (2016) Benchmarking DFT-GGA calculations for the structure optimisation of neutral-framework zeotypes. Theoretical Chemistry Accounts, 135, 257.

Fischer, M., Kim, W.J., Badawi, M., and Lebègue, S. (2019) Benchmarking the performance of approximate van der Waals methods for the structural and energetic properties of SiO 2 and AlPO 4 frameworks. Journal of Chemical Physics, 150.

Fletcher, R.E., Wells, S.A., Leung, K.M., Edwards, P.P., and Sartbaeva, A. (2015) Intrinsic flexibility of porous materials; theory, modelling and the flexibility window of the EMT zeolite framework. Acta Crystallographica Section B Structural Science, Crystal Engineering and Materials, 71, 641–647.

Fois, E., and Tabacchi, G. (2019) Water in zeolite L and its MOF mimic. Zeitschrift fur Kristallographie - Crystalline Materials, DOI: 10.1515/zkri-2018-2153

Fois, E., Gamba, A., and Tabacchi, G. (1998) Structure and Dynamics of a Brønsted Acid Site in a Zeolite: An ab Initio Study of Hydrogen Sodalite. The Journal of Physical Chemistry B, 102, 3974–3979.

——— (1999) Ab initio molecular dynamics study of the Brnsted acid site in a gallium zeolite.

621 Physical Chemistry Chemical Physics, 1, 531–536.

622 ——— (2000) First-principles simulation of the intracage oxidation of nitrite to nitrate sodalite.
623 Chemical Physics Letters, 329, 1–6.

624 Fois, E., Gamba, A., Tabacchi, G., Coluccia, S., and Martra, G. (2003) Ab Initio Study of Defect Sites
625 at the Inner Surfaces of Mesoporous Silicas. The Journal of Physical Chemistry B, 107, 10767–
626 10772.

627 Fois, E., Gamba, A., Tabacchi, G., Arletti, R., Quartieri, S., and Vezzalini, G. (2005) The "template"
628 effect of the extra-framework content on zeolite compression: The case of yugawaralite. American
629 Mineralogist, 90, 28–35.

630 Fois, E., Gamba, A., and Tabacchi, G. (2008a) Bathochromic effects in electronic excitation spectra of
631 hydrated Ti zeolites: A theoretical characterization. ChemPhysChem, 9, 538–543.

632 Fois, E., Gamba, A., Tabacchi, G., and Trudu, F. (2008b) First principles studies on boron sites.
633 Studies in Surface Science and Catalysis, 174, 751–754.

634 Fois, E., Gamba, A., Trudu, F., and Tabacchi, G. (2008c) H2O-induced trigonal-to-tetrahedral
635 transition in boron zeolites. Nuovo Cimento della Societa Italiana di Fisica B, 123, 1567–1574.

636 Fois, E., Gamba, A., Medici, C., Tabacchi, G., Quartieri, S., Mazzucato, E., Arletti, R., Vezzalini, G.,
637 and Dmitriev, V. (2008d) High pressure deformation mechanism of Li-ABW: Synchrotron XRPD
638 study and ab initio molecular dynamics simulations. Microporous and Mesoporous Materials, 115,
639 267–280.

640 Fois, E., Tabacchi, G., Barreca, D., Gasparotto, A., and Tondello, E. (2010a) "Hot" surface activation
641 of molecular complexes: Insight from modeling studies. Angewandte Chemie - International

642 Edition, 49, 1944–1948.

643 Fois, E., Tabacchi, G., and Calzaferri, G. (2010b) Interactions, behavior, and stability of fluorenone
644 inside zeolite nanochannels. Journal of Physical Chemistry C, 114, 10572–10579.

645 ——— (2012) Orientation and order of xanthene dyes in the one-dimensional channels of zeolite L:
646 Bridging the gap between experimental data and molecular behavior. Journal of Physical
647 Chemistry C, 116, 16784–16799.

648 Fois, E., Tabacchi, G., Devaux, A., Belser, P., Brühwiler, D., and Calzaferri, G. (2013) Host-guest
649 interactions and orientation of dyes in the one-dimensional channels of zeolite L. Langmuir, 29,
650 9188–9198.

651 Formalik, F., Fischer, M., Rogacka, J., Firlej, L., and Kuchta, B. (2018) Benchmarking of GGA density
652 functionals for modeling structures of nanoporous, rigid and flexible MOFs. The Journal of
653 Chemical Physics, 149, 064110.

654 Fraux, G., Coudert, F.-X., Boutin, A., and Fuchs, A.H. (2017) Forced intrusion of water and aqueous
655 solutions in microporous materials: from fundamental thermodynamics to energy storage devices.
656 Chem. Soc. Rev., 46, 7421–7437.

657 Gaigeot, M.-P., and Sulpizi, M. (2016) Mineral-Water Interaction. In Molecular Modeling of
658 Geochemical Reactions pp. 271–309. John Wiley & Sons, Ltd, Chichester, UK.

659 Gatta, G.D. (2008) Does porous mean soft? On the elastic behaviour and structural evolution of zeolites
660 under pressure. Zeitschrift fur Kristallographie, 223, 160–170.

661 Gatta, G.D., and Lee, Y. (2014) Zeolites at high pressure: A review. Mineralogical Magazine, 78, 267–
662 291.

Gatta, G.D., Sartbaeva, A., and Wells, S.A. (2009) Compression behaviour and flexibility window of the analcime-like feldspathoids: experimental and theoretical findings. European Journal of Mineralogy, 21, 571–580.

Gatta, G.D., Angel, R.J., Zhao, J., Alvaro, M., Rotiroti, N., and Carpenter, M.A. (2011) Phase stability, elastic behavior, and pressure-induced structural evolution of kalsilite: A ceramic material and high-T/high-P mineral. American Mineralogist, 96, 1363–1372.

Gatta, G.D., Tabacchi, G., Fois, E., and Lee, Y. (2016) Behaviour at high pressure of Rb7NaGa8Si12O40·3H2O (a zeolite with EDI topology): a combined experimental–computational study. Physics and Chemistry of Minerals, 43, 209–216.

Gatta, G.D., Lotti, P., and Tabacchi, G. (2018) The effect of pressure on open-framework silicates: elastic behaviour and crystal–fluid interaction. Physics and Chemistry of Minerals, 45, 115–138.

Giannozzi, P., Baroni, S., Bonini, N., Calandra, M., Car, R., Cavazzoni, C., Ceresoli, D., Chiarotti, G.L., Cococcioni, M., Dabo, I., and others (2009) QUANTUM ESPRESSO: a modular and open-source software project for quantum simulations of materials. Journal of Physics: Condensed Matter, 21, 395502.

Giannozzi, P., Andreussi, O., Brumme, T., Bunau, O., Buongiorno Nardelli, M., Calandra, M., Car, R., Cavazzoni, C., Ceresoli, D., Cococcioni, M., and others (2017) Advanced capabilities for materials modelling with Quantum ESPRESSO. Journal of Physics: Condensed Matter, 29, 465901.

Gigli, L., Arletti, R., Tabacchi, G., Fois, E., Vitillo, J.G., Martra, G., Agostini, G., Quartieri, S., and Vezzalini, G. (2014) Close-Packed Dye Molecules in Zeolite Channels Self-Assemble into Supramolecular Nanoladders. The Journal of Physical Chemistry C, 118, 15732–15743.

685 Gigli, L., Arletti, R., Tabacchi, G., Fabbiani, M., Vitillo, J.G., Martra, G., Devaux, A., Miletto, I.,
686 Quartieri, S., Calzaferri, G., and others (2018a) Structure and Host–Guest Interactions of
687 Perylene–Diimide Dyes in Zeolite L Nanochannels. The Journal of Physical Chemistry C, 122,
688 3401–3418.

689 Gigli, L., Arletti, R., Fois, E., Tabacchi, G., Quartieri, S., Dmitriev, V., and Vezzalini, G. (2018b)
690 Unravelling the High-Pressure Behaviour of Dye-Zeolite L Hybrid Materials. Crystals, 8, 79.

691 Gigli, L., Vezzalini, G., Quartieri, S., and Arletti, R. (2019) Compressibility behavior and pressure-
692 induced over-hydration of zeolite K–AlSi-L. Microporous and Mesoporous Materials, 276, 160–
693 166.

694 Giustetto, R., Seenivasan, K., Bonino, F., Ricchiardi, G., Bordiga, S., Chierotti, M.R., and Gobetto, R.
695 (2011) Host/guest interactions in a sepiolite-based maya blue pigment: A spectroscopic study.
696 Journal of Physical Chemistry C, 115, 16764–16776.

697 Gottardi, G., and Galli, E. (2012) Natural Zeolites, 412 p. Springer Berlin Heidelberg.

698 Grajciar, L., Areán, C.O., Pulido, A., and Nachtigall, P. (2010) Periodic DFT investigation of the effect
699 of aluminium content on the properties of the acid zeolite H-FER. Physical chemistry chemical
700 physics : PCCP, 12, 1497–506.

701 Grimme, S. (2006) Semiempirical GGA-type density functional constructed with a long-range
702 dispersion correction. Journal of Computational Chemistry, 27, 1787–1799.

703 Guo, G., Long, Y., and Sun, Y. (2000) Synthesis of FER type zeolite with tetrahydrofuran as the
704 template. Chemical Communications, 0, 1893–1894.

705 Hay, H., Ferlat, G., Casula, M., Seitsonen, A.P., and Mauri, F. (2015) Dispersion effects in SiO 2

706 polymorphs: An ab initio study. PHYSICAL REVIEW B, 92, 144111.

707 Hoover, W.G. (1985) Canonical dynamics: Equilibrium phase-space distributions. Physical Review A,
708 31, 1695–1697.

709 Humphrey, W., Dalke, A., and Schulten, K. (1996) VMD: Visual molecular dynamics. Journal of
710 Molecular Graphics, 14, 33–38.

711 IBM Corp. 1990–2017, and MPI für Festkörperforschung Stuttgart 1997–2001 (2017) CPMD: Car
712 Parrinello Molecular Dynamics.

713 Insuwan, W., Rangsriwatananon, K., Meeprasert, J., Namuangruk, S., Surakhot, Y., Kungwan, N., and
714 Jungsuttiwong, S. (2017) Combined experimental and theoretical investigation on Fluorescence
715 Resonance Energy Transfer of dye loaded on LTL zeolite. Microporous and Mesoporous
716 Materials, 241, 372–382.

717 Jordá, J.L., Rey, F., Sastre, G., Valencia, S., Palomino, M., Corma, A., Segura, A., Errandonea, D.,
718 Lacomba, R., Manjón, F.J., and others (2013) Synthesis of a Novel Zeolite through a Pressure-
719 Induced Reconstructive Phase Transition Process. Angewandte Chemie, 125, 10652–10656.

720 Ke, Q., Sun, T., Wei, X., Guo, Y., Xu, S., and Wang, S. (2019) Economical synthesis strategy of RHO
721 zeolites with fine-tuned composition and porosity for enhanced trace CO2 capture. Chemical
722 Engineering Journal, 359, 344–353.

723 Kim, Y., Choi, J., Vogt, T., and Lee, Y. (2018) Structuration under pressure: Spatial separation of
724 inserted water during pressure-induced hydration in mesolite. American Mineralogist, 103, 175–
725 178.

726 Kleinman, L., and Bylander, D.M. (1982) Efficacious form for model pseudopotentials. Physical

727 Review Letters, 48, 1425–1428.

728 Kong, M., Lee, Yongmoon, Gatta, G.D., and Lee, Yongjae (2018) Comparative compressional
729 behavior of chabazite with Li+, Na+, Ag+, K+, Rb+, and Cs+ as extra-framework cations.
730 American Mineralogist, 103, 207–215.

731 Kraus, P., and Frank, I. (2017) On the dynamics of H_2 adsorption on the Pt(111) surface. International
732 Journal of Quantum Chemistry, 117, e25407.

733 Kremleva, A., Vogt, T., and Rösch, N. (2013) Monovalent cation-exchanged natrolites and their
734 behavior under pressure. A computational study. Journal of Physical Chemistry C, 117, 19020–
735 19030.

736 ——— (2014) Potassium-exchanged natrolite under pressure. computational study vs experiment.
737 Journal of Physical Chemistry C, 118, 22030–22039.

738 Kubicki, J.D. (2016) Molecular Modeling of Geochemical Reactions: An Introduction, 440 p. (J.D.
739 Kubicki, Ed.). John Wiley & Sons, Ltd.

740 Kuperman, A., Nadimi, S., Oliver, S., Ozin, G.A., Garcés, J.M., and Olken, M.M. (1993) Non-aqueous
741 synthesis of giant crystals of zeolites and molecular sieves. Nature, 365, 239–242.

742 Levien, L., and Prewitt, C. (1981) High-pressure crystal structure and compressibility of coesite.
743 American Mineralogist, 66, 324–333.

744 Lewis, J.E., Freyhardt, C.C., and Davis, M.E. (1996) Location of Pyridine Guest Molecules in an
745 Electroneutral { 3 ∞ }[SiO 4/2] Host Framework: Single-Crystal Structures of the As-Synthesized
746 and Calcined Forms of High-Silica Ferrierite. The Journal of Physical Chemistry, 100, 5039–
747 5049.

748 Li, G., and Pidko, E.A. (2019) The nature and catalytic function of cation sites in zeolites: a
749 computational perspective The nature and catalytic function of cation sites in zeolites: a
750 computational perspective. ChemCatChem, 11, 134–156.

751 Li, H., and Li, P. (2018) Luminescent materials of lanthanoid complexes hosted in zeolites. Chemical
752 Communications, 54, 13884–13893.

753 Liang, Y., Miranda, C.R., and Scandolo, S. (2007) Tuning oxygen packing in silica by nonhydrostatic
754 pressure. Physical Review Letters, 99, 1–4.

755 Liebau, F. (1961) Untersuchungen über die Grösse des Si–O–Si-Valenzwinkels. Acta
756 Crystallographica, 14, 1103–1109.

757 Liebau, F. (1985) Structural Chemistry of Silicates, 347 p. Springer Verlag, Berlin, Heidelberg, New
758 York, Tokyo.

759 Lotti, P., Gatta, G.D., Merlini, M., and Hanfland, M. (2014) High-pressure behavior of davyne [CAN-
760 topology]: An in situ single-crystal synchrotron diffraction study. Microporous and Mesoporous
761 Materials, 198, 203–214.

762 Lotti, P., Arletti, R., Gatta, G.D., Quartieri, S., Vezzalini, G., Merlini, M., Dmitriev, V., and Hanfland,
763 M. (2015) Compressibility and crystal-fluid interactions in all-silica ferrierite at high pressure.
764 Microporous and Mesoporous Materials, 218, 42–54.

765 Lotti, P., Gatta, G.D., Comboni, D., Merlini, M., Pastero, L., and Hanfland, M. (2016) AlPO4-5 zeolite
766 at high pressure: Crystal-fluid interaction and elastic behavior. Microporous and Mesoporous
767 Materials, 228, 158–167.

768 Luo, H.Y., Lewis, J.D., and Román-Leshkov, Y. (2016) Lewis Acid Zeolites for Biomass Conversion:

769 Perspectives and Challenges on Reactivity, Synthesis, and Stability. Annual Review of Chemical
770 and Biomolecular Engineering, 7, 663–692.

771 Manzano, H., Gartzia-Rivero, L., Bañuelos, J., and López-Arbeloa, I. (2013) Ultraviolet-visible dual
772 absorption by single BODIPY dye confined in LTL zeolite nanochannels. Journal of Physical
773 Chemistry C, 117, 13331–13336.

774 Marqueño, T., Santamaria-Perez, D., Ruiz-Fuertes, J., Chuliá-Jordán, R., Jordá, J.L., Rey, F., McGuire,
775 C., Kavner, A., MacLeod, S., Daisenberger, D., and others (2018) An Ultrahigh CO_2 -Loaded
776 Silicalite-1 Zeolite: Structural Stability and Physical Properties at High Pressures and
777 Temperatures. Inorganic Chemistry, 57, 6447–6455.

778 Martínez-Suarez, L., Siemer, N., Frenzel, J., and Marx, D. (2015) Reaction Network of Methanol
779 Synthesis over Cu/ZnO Nanocatalysts. ACS Catalysis, 5, 4201–4218.

780 Marx, D., and Hutter, J. (2009) Ab Initio Molecular Dynamics. Cambridge University Press,
781 Cambridge.

782 Matthew, G.T., Matthew, P.S., Martin, T.D., and David, A.K. (2001) Dynamic structural disorder in
783 cristobalite: neutron total scattering measurement and reverse Monte Carlo modelling. Journal of
784 Physics: Condensed Matter, 13, 403.

785 Montejo-Valencia, B.D., and Curet-Arana, M.C. (2015) DFT Study of the Lewis Acidities and Relative
786 Hydrothermal Stabilities of BEC and BEA Zeolites Substituted with Ti, Sn, and Ge. The Journal
787 of Physical Chemistry C, 119, 4148–4157.

788 Morris, R.E., Weigel, S.J., Henson, N.J., Bull, L.M., Cheetham, A.K., Janicke, M.T., and Chmelka,
789 B.F. (1994) A Synchrotron X-ray Diffraction, Neutron Diffraction,29Si MAS-NMR, and

790 Computational Study of the Siliceous Form of Zeolite Ferrierite. Journal of the American
791 Chemical Society, 116, 11849–11855.

792 Nachtigall, P., Bludský, O., Grajciar, L., Nachtigallová, D., Delgado, M.R., and Areán, C.O. (2009)
793 Computational and FTIR spectroscopic studies on carbon monoxide and dinitrogen adsorption on
794 a high-silica H-FER zeolite. Physical Chemistry Chemical Physics, 11, 791–802.

795 Nie, X., Ji, X., Chen, Y., Guo, X., and Song, C. (2017) Mechanistic investigation of propylene
796 epoxidation with H2O2 over TS-1: Active site formation, intermediate identification, and oxygen
797 transfer pathway. Molecular Catalysis, 441, 150–167.

798 Nosé, S. (1984) A unified formulation of the constant temperature molecular dynamics methods. The
799 Journal of Chemical Physics, 81, 511–519.

800 Paul, G., Bisio, C., Braschi, I., Cossi, M., Gatti, G., Gianotti, E., and Marchese, L. (2018) Combined
801 solid-state NMR, FT-IR and computational studies on layered and porous materials. Chemical
802 Society Reviews, 47, 5684–5739.

803 Perdew, J.P., Burke, K., and Ernzerhof, M. (1996) Generalized Gradient Approximation Made Simple.
804 Physical Review Letters, 77, 3865–3868.

805 Pintus, A.M., Gabrieli, A., Pazzona, F.G., Pireddu, G., and Demontis, P. (2019) Molecular QCA
806 embedding in microporous materials. Physical Chemistry Chemical Physics, 21, 7879–7884.

807 Prinsen, P., and Luque, R. (2019) Chapter 1. Introduction to Nanocatalysts, in: Nanoparticle Design
808 and Characterization for Catalytic Applications in Sustainable Chemistry, The Royal Society of
809 Chemistry, pp. 1–36. DOI: 10.1039/9781788016292-00001

810 Redondo, A., and Hay, P.J. (1993) Quantum chemical studies of acid sites in zeolite ZSM-5. The

811 Journal of Physical Chemistry, 97, 11754–11761.

812 Richet, P., and Ottonello, G. (2014) The Earth as a multiscale quantum-mechanical system. Comptes
813 Rendus - Geoscience, 346, 317–325.

814 Román-Román, E.I., and Zicovich-Wilson, C.M. (2015) The role of long-range van der Waals forces in
815 the relative stability of SiO2-zeolites. Chemical Physics Letters, 619, 109–114.

816 Santoro, M., Scelta, D., Dziubek, K., Ceppatelli, M., Gorelli, F.A., Bini, R., Garbarino, G., Thibaud,
817 J.M., Di Renzo, F., Cambon, O., and others (2016) Synthesis of 1D Polymer/Zeolite
818 Nanocomposites under High Pressure. Chemistry of Materials, 28, 4065–4071.

819 Sartbaeva, A., Wells, S.A., Redfern, S.A.T., Hinton, R.W., and Reed, S.J.B. (2005) Ionic diffusion in
820 quartz studied by transport measurements, SIMS and atomistic simulations. Journal of Physics
821 Condensed Matter, 17, 1099–1112.

822 Sartbaeva, A., Gatta, G.D., and Wells, S.A. (2008) Flexibility window controls pressure-induced phase
823 transition in analcime. Europhysics Letters, 83, 26002.

824 Seryotkin, Y. V. (2019) Evolution of the brewsterite structure at high pressure: A single-crystal X-ray
825 diffraction study. Microporous and Mesoporous Materials, 276, 167–172.

826 Seryotkin, Y. V., and Bakakin, V. V. (2018) Structure of K-Substituted Zeolite Clinoptillolite and Its
827 Behavior Upon Compression in Penetrating and Non-Penetrating Media. Journal of Structural
828 Chemistry, 59, 1392–1399.

829 Signorile, M., Damin, A., Bonino, F., Crocellà, V., Ricchiardi, G., Lamberti, C., and Bordiga, S. (2018)
830 Computational Assessment of Relative Sites Stabilities and Site-Specific Adsorptive Properties of
831 Titanium Silicalite-1. Journal of Physical Chemistry C, 122, 1612–1621.

832 Sirijaraensre, J., and Limtrakul, J. (2013) Mechanisms of the ammonia oxidation by hydrogen peroxide
833 over the perfect and defective Ti species of TS-1 zeolite. Physical Chemistry Chemical Physics,
834 15, 18093.

835 Spanó, E., Tabacchi, G., Gamba, A., and Fois, E. (2006) On the role of Ti(IV) as a lewis acid in the
836 chemistry of titanium zeolites: Formation, structure, reactivity, and aging of ti-peroxo oxidizing
837 intermediates. A first principles study. Journal of Physical Chemistry B, 110, 21651–21661.

838 Spearing, D.R., Farnan, I., and Stebbins, J.F. (1992) Dynamics of the α-β phase transitions in quartz
839 and cristobalite as observed by in-situ high temperature 29Si and 17O NMR. Physics and
840 Chemistry of Minerals, 19, 307–321.

841 Swainson, I.P., and Dove, M.T. (1993) Low-frequency floppy modes in -cristobalite. Physical Review
842 Letters, 71, 193–196.

843 Tabacchi, G. (2018) Supramolecular Organization in Confined Nanospaces. ChemPhysChem, 19,
844 1249–1297.

845 Tabacchi, G., Gianotti, E., Fois, E., Martra, G., Marchese, L., Coluccia, S., and Gamba, A. (2007)
846 Understanding the vibrational and electronic features of Ti(IV) sites in mesoporous silicas by
847 integrated Ab initio and spectroscopic investigations. Journal of Physical Chemistry C, 111, 4946–
848 4955.

849 Tabacchi, G., Fois, E., Barreca, D., and Gasparotto, A. (2014a) CVD precursors for transition metal
850 oxide nanostructures: molecular properties, surface behavior and temperature effects. physica
851 status solidi (a), 211, 251–259.

852 ——— (2014b) Opening the Pandora's jar of molecule-to-material conversion in chemical vapor

deposition: Insights from theory. International Journal of Quantum Chemistry, 114, 1–7.

Tabacchi, G., Fois, E., and Calzaferri, G. (2015) Structure of Nanochannel Entrances in Stopcock-Functionalized Zeolite L Composites. Angewandte Chemie International Edition, 54, 11112–11116.

Tabacchi, G., Silvi, S., Venturi, M., Credi, A., and Fois, E. (2016a) Dethreading of a Photoactive Azobenzene-Containing Molecular Axle from a Crown Ether Ring: A Computational Investigation. ChemPhysChem, 17, 1913–1919.

Tabacchi, G., Calzaferri, G., and Fois, E. (2016b) One-dimensional self-assembly of perylene-diimide dyes by unidirectional transit of zeolite channel openings. Chem. Commun., 52, 11195–11198.

Torres, C., Gulín-González, J., Navas-Conyedo, E., Demontis, P., and Suffritti, G.B. (2013) The behavior of silicalite-1 under high pressure conditions studied by computational simulation. Structural Chemistry, 24, 909–915.

Tran, F., Stelzl, J., and Blaha, P. (2016) Rungs 1 to 4 of DFT Jacob's ladder: Extensive test on the lattice constant, bulk modulus, and cohesive energy of solids. The Journal of Chemical Physics, 144, 204120.

Troullier, N., and Martins, J.L. (1991) Efficient pseudopotentials for plane-wave calculations. Physical Review B, 43, 1993–2006.

Trudu, F., Tabacchi, G., Gamba, A., and Fois, E. (2007) First principles studies on boron sites in zeolites. Journal of Physical Chemistry A, 111, 11626–37.

——— (2008) Water in Acid Boralites: Hydration Effects on Framework B Sites. The Journal of Physical Chemistry C, 112, 15394–15401.

Tuma, C., and Sauer, J. (2006) Treating dispersion effects in extended systems by hybrid MP2:DFT calculations - Protonation of isobutene in zeolite ferrierite. Physical Chemistry Chemical Physics, 8, 3955–3965.

Ugliengo, P., Busco, C., Civalleri, B., and Zicovich-Wilson, C.M. (2005) Carbon monoxide adsorption on alkali and proton-exchanged chabazite: An ab-initio periodic study using the CRYSTAL code. In Molecular Physics Vol. 103, pp. 2559–2571. Taylor & Francis Group.

Van Speybroeck, V., Hemelsoet, K., Joos, L., Waroquier, M., Bell, R.G., and Catlow, C.R.A. (2015) Advances in theory and their application within the field of zeolite chemistry. Chem. Soc. Rev., 44, 7044–7111.

Vanderbilt, D. (1990) Soft self-consistent pseudopotentials in a generalized eigenvalue formalism. Physical Review B, 41, 7892–7895.

Vaughan, P.A. (1966) The crystal structure of the zeolite ferrierite. Acta Crystallographica, 21, 983–990.

Vezzalini, G., Quartieri, S., Galli, E., Alberti, A., Cruciani, G., and Kvick, A. (1997) Crystal structure of the zeolite mutinaite, the natural analog of ZSM-5. Zeolites, 19, 323–325.

Vezzalini, G., Arletti, R., and Quartieri, S. (2014) High-pressure-induced structural changes, amorphization and molecule penetration in MFI microporous materials: A review. Acta Crystallographica Section B: Structural Science, Crystal Engineering and Materials, 70, 444–451.

Viani, L., Minoia, A., Cornil, J., Beljonne, D., Egelhaaf, H.J., and Gierschner, J. (2016) Resonant energy transport in dye-filled monolithic crystals of zeolite L: Modeling of inhomogeneity. Journal of Physical Chemistry C, 120, 27192–27199.

Wang, C., Bai, P., Siepmann, J.I., and Clark, A.E. (2014) Deconstructing Hydrogen-Bond Networks in Con fi ned Nanoporous Materials: Implications for Alcohol − Water Separation. The Journal of Physical Chemistry C, 118, 19723–19732.

Wang, H., Deng, Y., and Zhou, R. (2018a) Aromatic sulfur compounds oxidation with H2O2 over fully coordinated and defect sites in Ti-beta zeolites: evaluation by density functional theory. Theoretical Chemistry Accounts, 137, 66.

Wang, H., Zhou, R., and Deng, Y. (2018b) Thiophene oxidation with H2O2over defect and perfect titanium silicalite-1: a computational study. Reaction Kinetics, Mechanisms and Catalysis, 124, 45–60.

Wells, S.A., and Sartbaeva, A. (2012) Template-Based Geometric Simulation of Flexible Frameworks. Materials, 5, 415–431.

Wells, S.A., Dove, M.T., Tucker, M.G., and Trachenko, K. (2002) Real-space rigid-unit-mode analysis of dynamic disorder in quartz, cristobalite and amorphous silica. Journal of Physics Condensed Matter, 14, 4645–4657.

Wells, S.A., Sartbaeva, A., and Gatta, G.D. (2011) Flexibility windows and phase transitions of ordered and disordered ANA framework zeolites. EPL (Europhysics Letters), 94, 56001.

Wells, S.A., Leung, K.M., Edwards, P.P., and Sartbaeva, A. (2015) Flexibility windows in faujasite with explicit water and methanol extra-framework content. Dalton Transactions, 44, 5978–5984.

White, C.L.I.M., Ruiz-Salvador, A.R., and Lewis, D.W. (2004) Pressure-Induced Hydration Effects in the Zeolite Laumontite. Angewandte Chemie - International Edition, 43, 469–472.

Wiedemann, S.C.C., Ristanovic, Z., Whiting, G.T., Reddy Marthala, V.R., Kärger, J., Weitkamp, J.,

916 Wels, B., Bruijnincx, P.C.A., and Weckhuysen, B.M. (2016) Large Ferrierite Crystals as Models
917 for Catalyst Deactivation during Skeletal Isomerisation of Oleic Acid: Evidence for Pore Mouth
918 Catalysis. Chemistry - A European Journal, 22, 199–210.

919 Woodtli, P., Giger, S., Müller, P., Sägesser, L., Zucchetto, N., Reber, M.J., Ecker, A., and Brühwiler,
920 D. (2018) Indigo in the nanochannels of zeolite L: Towards a new type of colorant. Dyes and
921 Pigments, 149, 456–461.

922 Yokomori, Y., Wachsmuth, J., and Nishi, K. (2001) Structure and Brønsted acid sites of ferrierite.
923 Microporous and Mesoporous Materials, 50, 137–143.

924 Zendehdel, M., Bodaghifard, M.A., Behyar, H., and Mortezaei, Z. (2018) Alkylaminopyridine-grafted
925 on HY Zeolite: Preparation, characterization and application in synthesis of 4 H -Chromenes.
926 Microporous and Mesoporous Materials, 266, 83–89.

927 Zhou, X., Wesolowski, T.A., Tabacchi, G., Fois, E., Calzaferri, G., and Devaux, A. (2013) First-
928 principles simulation of the absorption bands of fluorenone in zeolite L. Phys. Chem. Chem.
929 Phys., 15, 159–167.

930

931

LIST OF CAPTIONS OF FIGURES

Figure 1. Optimized structure of *Pmnn* Si-FER with atom labels. Solid lines represent simulation cell.

Figure 2. Optimized structure of *Immm* Si-FER with atom labels. Solid lines represent simulation cell.

Figure 3. Instantaneous positions of the Si1, O4, Si1 centers sampled along the FPMD simulation at 60 fs time intervals (dots) superposed to the average structure of Si-FER *Immm* obtained from the time-average of the atomic positions (grey sticks).

DEPOSIT ITEMS

Supporting information pdf file; cif file of the optimized *Immm*-SI-FER (Fer_Immm_opt_60_360.cif) ; cif file of the optimized structure of *Pmnn* Si-FER (Fer_Pnnm_opt_60_360.cif); cif file of the time-average of the atomic positions from FPMD simulation of *Immm*-SI-FER at 438 K (Fer_Immm_FPMD_438K.cif); cif files of the structures including displacements associated to Mode1, Mode2, Mode3, Mode4. These deposit items are also available in the ChemRxiv repository under the link **https://doi.org/10.26434/chemrxiv.7746371.v2**.

TABLES

Table 1. Optimized lattice parameters calculated for Si-FER *Immm* (orthorhombic, SG=71) and Si-FER *Pmnn* (orthorhombic SG=58).

	Immm	*Immm**	*Pmnn*	*Pmnn* (a)	*Pmnn* (b)	*Pmnn* (c)	*Pmnn* (d)
a / Å	**19.0332**	19.0180	**18.7164**	18.7144	18.692	18.7202	18.713
b / Å	**14.2565**	14.3030	**14.1285**	14.1226	14.157	14.07025	14.070
c / Å	**7.5254**	7.5410	**7.4312**	7.4281	7.440	7.41971	7.418
V / Å^3	**2042.00**	2051.26	**1965.06**	1963.22	1968.48	1954.32	1953.1

*From the IZA-SC database of Zeolite Structures, C. Baerlocker and L.B. McCusker, http://www.iza-structure.org/database; (a) From Ref. (Fischer et al. 2016); (b) From ref. (Hay et al. 2015); c) from ref. (Morris et al. 1994); (d) From Ref.(Lewis et al. 1996).

Table 2. Space group (SG), energy difference with respect to Si-FER *Pmnn* (ΔE), and value of the Si1-O4-Si1 angle for the structures obtained from geometry optimization along Mode1, Mode2, Mode3, Mode4. The values for Si-FER *Immm* and Si-FER *Pmnn* are included for comparison.[a]

	Immm	*Opt-Mode1*	*Opt-Mode2*	*Opt-Mode3*	*Opt-Mode4*	*Pmnn*[b]
SG	71	12 (*C2/m*)	44 (*I2mm*)	44 (*Imm2*)	44 (*I2mm*)	58
ΔE / kcal/mol	0.154	0.070	0.083	0.092	0.119	0
Si1-O4-Si1 / º	180	180	165.4	166.1	172.2	158.7

[a] All calculations performed with CPMD (30/240 PW cutoff). Energy differences per formula units are calculated with respect to the *Pmnn* minimum energy structure. [b]For *Pmnn*, the angle corresponding to the *Immm* Si1-O4-Si1 angle is labeled Si1-O8-Si2.

FIGURES

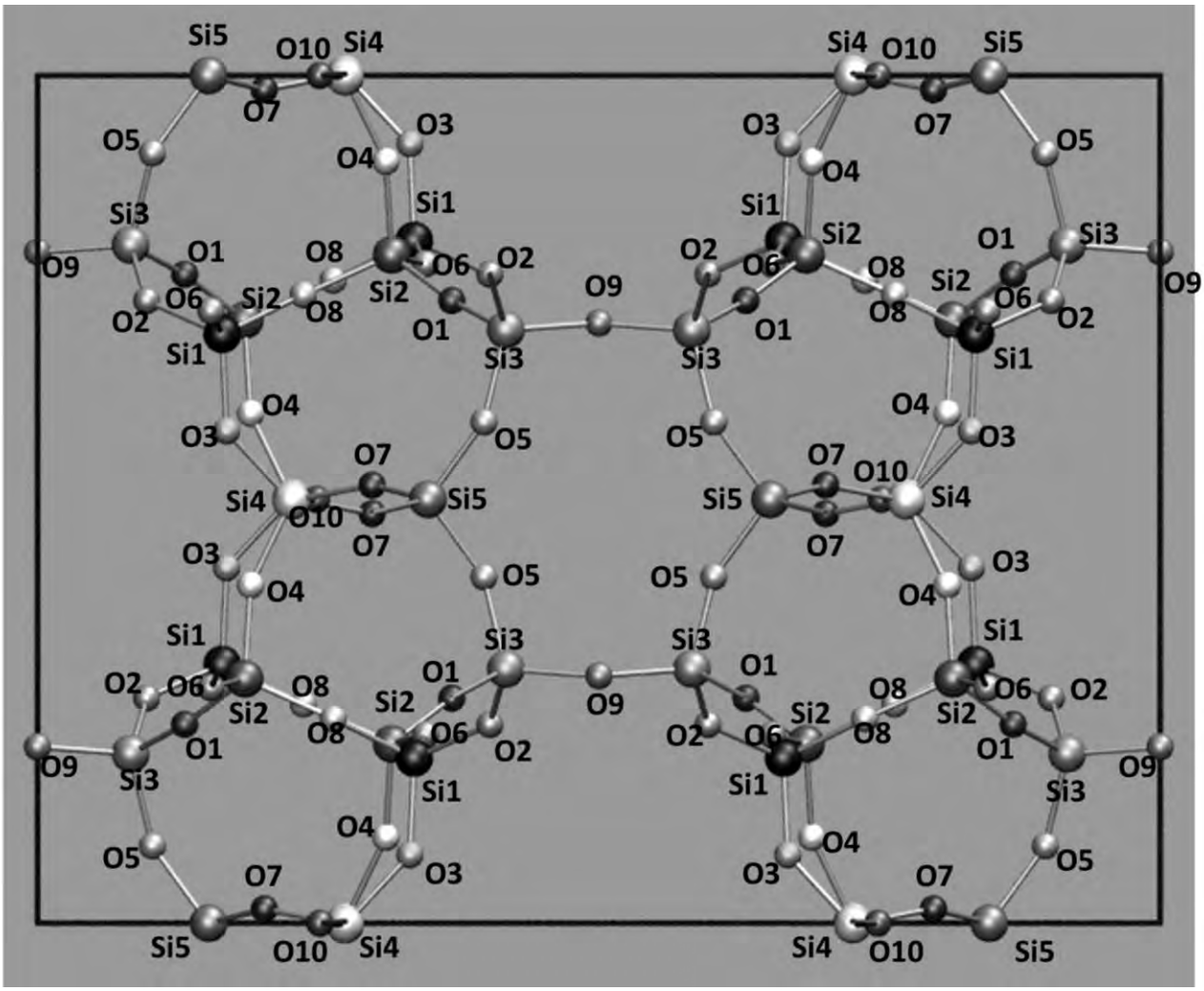

962

963 **Figure 1.**

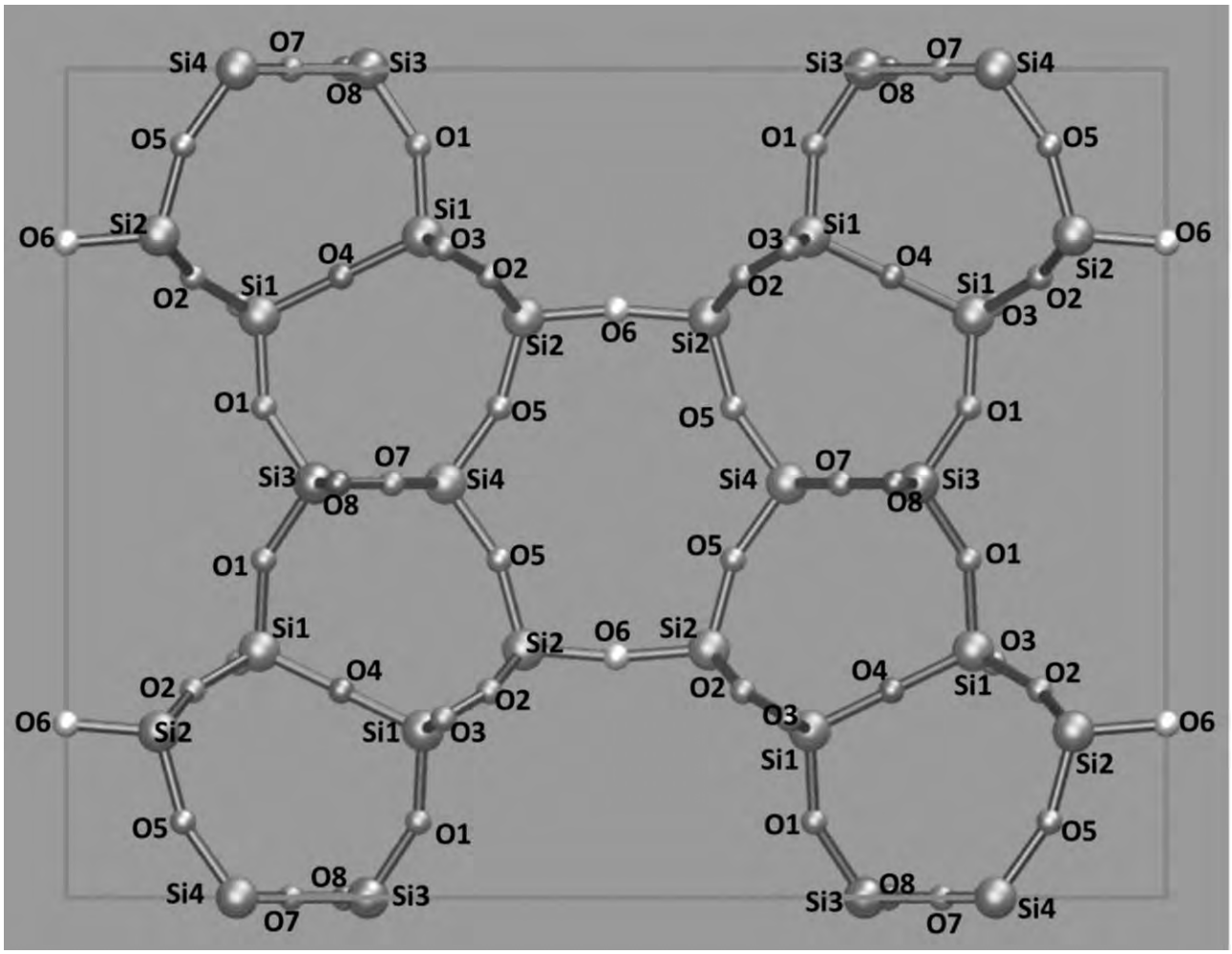

964

965 **Figure 2.**

966

967 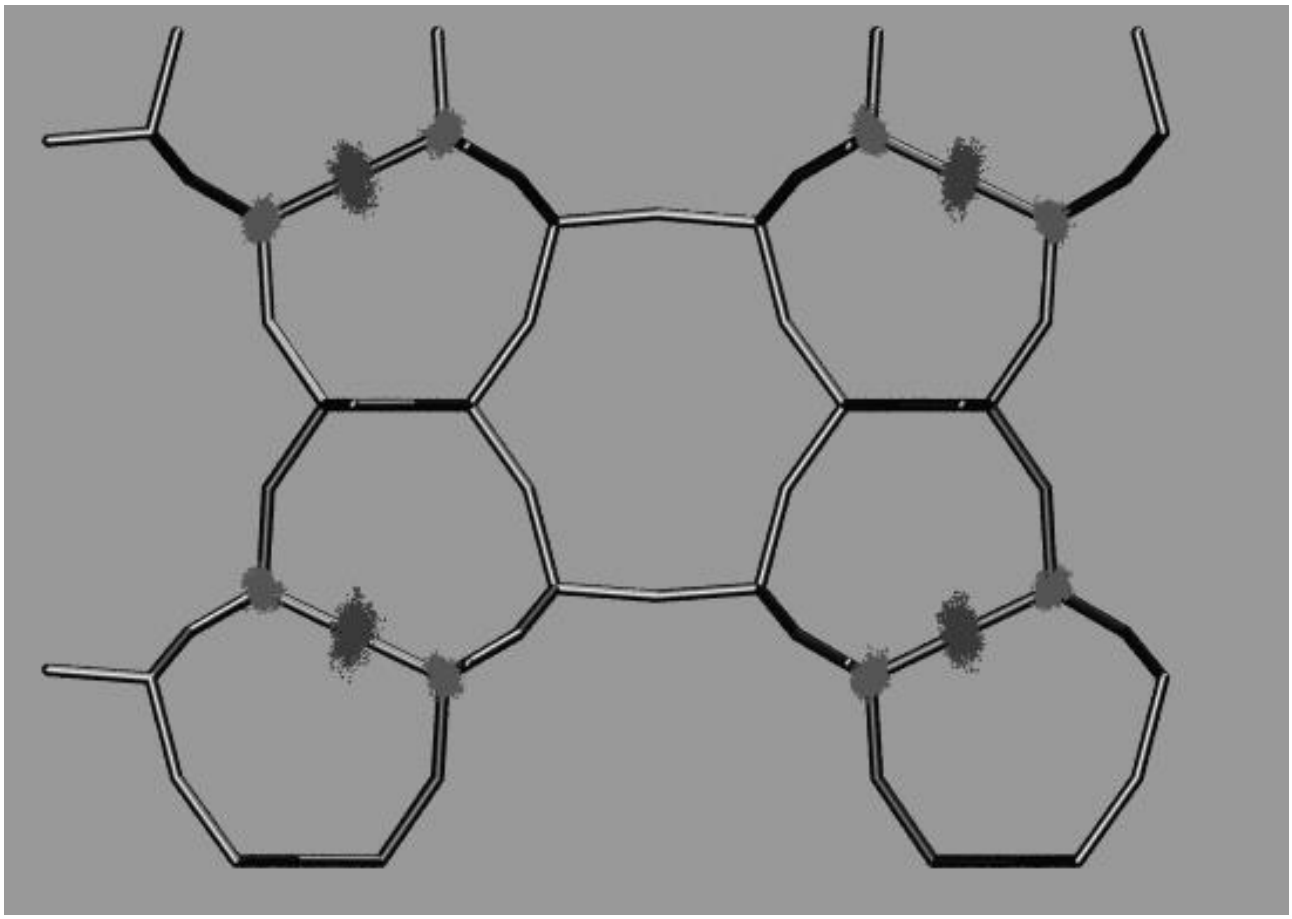

968 **Figure 3.**

969